Gas-Phase Fragmentation of Long-Lived Cysteine Radical Cations Formed Via NO Loss from Protonated S-Nitrosocysteine*,†

Victor Ryzhov,[a] Adrian K. Y. Lam,[b,c,d] and Richard A. J. O'Hair[b,c,d]

[a] Department of Chemistry and Biochemistry, Northern Illinois University, DeKalb, Illinois, USA
[b] School of Chemistry, The University of Melbourne, Melbourne, Victoria, Australia
[c] Bio21 Institute of Molecular Science and Biotechnology, The University of Melbourne, Melbourne, Victoria, Australia
[d] ARC Centre of Excellence for Free Radical Chemistry and Biotechnology, School of Chemistry, University of Melbourne, Melbourne, Victoria, Australia

In this work, we describe two different methods for generating protonated S-nitrosocysteine in the gas phase. The first method involves a gas-phase reaction of protonated cysteine with *t*-butylnitrite, while the second method uses a solution-based transnitrosylation reaction of cysteine with S-nitrosoglutathione followed by transfer of the resulting S-nitrosocysteine into the gas phase by electrospray ionization mass spectrometry (ESI-MS). Independent of the way it was formed, protonated S-nitrosocysteine readily fragments via bond homolysis to form a long-lived radical cation of cysteine ($Cys^{\bullet+}$), which fragments under collision-induced dissociation (CID) conditions via losses in the following relative abundance order: •COOH ⩾ CH_2S > $•CH_2SH$ ≈ H_2S. Deuterium labeling experiments were performed to study the mechanisms leading to these pathways. DFT calculations were also used to probe aspects of the fragmentation of protonated S-nitrosocysteine and the radical cation of cysteine. NO loss is found to be the lowest energy channel for the former ion, while the initially formed distonic $Cys^{\bullet+}$ with a sulfur radical site undergoes proton and/or H atom transfer reactions that precede the losses of CH_2S, •COOH, $•CH_2SH$, and H_2S. (J Am Soc Mass Spectrom 2009, 20, 985–995)

There has been renewed interest in the gas-phase formation and reactions of radical ions of biomolecules. The motivation for these studies range from fundamental interest in species related to biological processes such as enzyme catalysis [1] and oxidative chemistry associated with damage to biomolecules such as DNA [2] and proteins [3] through to the potential for developing novel mass spectrometry based analytical applications [4]. With regards to the formation of radical ions of amino acids and peptides, several methods have been developed as alternatives to electron ionization (EI) [5]. These include UV photodissociation [6–11] and ion-electron based techniques such as electron capture dissociation (ECD) [12–15]. Chemical-based methods that involve low-energy collision-induced dissociation (CID) [16] of ions generated via electrospray ionization and which can thus be carried out on a wide range of mass spectrometers, merit special discussion. The first, pioneered by Siu, involves carrying out CID of ternary metal complexes to form radical cations of peptides via the redox reaction shown in eq 1 [17–19]. To date, doubly charged copper(II) ternary metal complexes (eq 1, where Metal = Cu; L = a range of neutral ligands, x = 2, y = 0) and singly charged metal(III) complexes (eq 1, where Metal = Cr, Mn, Fe, and Co; L = a salen ligand, x = 3, y = 2) have been used to study the formation and reactions of peptide radical ions, including recent contributions from Julia Laskin [20–23].

$$[Metal^{x+}(L)^{y-}(M)]^{(x-y)+} \rightarrow [Metal^{(x-1)+}(L)^{y-}]^{(x-y-1)+} + M^{\bullet+} \quad (1)$$

The second method involves carrying out CID on a cationized peptide containing a functional group with a weak bond, which is susceptible to bond homolysis. A number of different functional groups have been examined to date including: (1) N-terminal azo derivatives [24]; (2) N-terminal [25] and lysine side-chain [26] carbamate derivatives; (3) serine nitrate ester deriva-

Address reprint requests to Dr. Richard O'Hair, AR Centre of Excellence for Free Radical Chemistry and Biotechnology, School of Chemistry, University of Melbourne, Parkville, Victoria 3010, Australia. E-mail: rohair@unimelb.edu.au

* Dedicated to our friend and collaborator Julia Laskin on the award of the Biemann Medal, which is in recognition for her outstanding contributions to mass spectrometry.

† Part 65 of the series "Gas-Phase Ion Chemistry of Biomolecules."

1044-0305/09/$32.00
doi:10.1016/j.jasms.2008.12.026

Published online January 9, 2009
Received November 18, 2008
Revised December 17, 2008
Accepted December 17, 2008

tives [27]; (4) S-nitrosocysteine derivatives [28]. These studies have opened up opportunities to examine the fundamental gas-phase chemistry of side-chain and backbone radical sites in peptides.

An important class of radicals in peptide chemistry are the side-chain thiolate radicals of cysteine residues, which are involved in a number of enzyme reactions [1], are implicated in protein damage [29] and in S–S and S–NO bond homolysis reactions in certain MS-based experiments [4, 28]. Recent work by Hao and Gross [28] has shown that the fragmentation of cysteine-based radicals of peptides yields information complementary to CID, similarly to ECD [12]. Since little is known about the mechanisms of these fragmentation reactions, it seemed desirable to have a detailed experimental and theoretical understanding of the CID behavior of the cysteine radical cation. Despite three theoretical studies on the fragmentation reactions of cysteine radical cations [30–32], experiments on long-lived radical cations of cysteine formed via alternative methods to EI have lagged behind. Attempts to generate radical cations of cysteine using Siu's method have failed [32, 33]. During studies aimed at extending the ion-molecule reactions of amino acid and peptide radical cations [27] to a range of other neutral reagents, we serendipitously discovered a nitrosylation reaction of protonated cysteine with *t*-butylnitrite which is related to reactions of simple thiols with nitroso compounds [34]. Here we use a combination of multistage mass spectrometry experiments, gas-phase ion-molecule reactions, solution phase transnitrosylation reactions, collision-induced dissociation, deuterium labeling, and density functional theory (DFT) calculations to study: (1) the formation of protonated S-nitrosocysteine; (2) the fragmentation reactions of protonated S-nitrosocysteine; (3) the fragmentation reactions of the cysteine radical cation.

Experimental

Materials

All purchased materials were used without further purification: cysteine (Cys), S-nitrosoglutathione (GSNO), and *t*-butylnitrite (90%) were from Sigma-Aldrich (Milwaukee, WI); d_2-cysteine, (99.5 atom % deuterium) and D_2O (99.9 atom % deuterium) were from Cambridge Isotope Laboratories (Andover, MA). Methanol (HPLC grade) and acetonitrile (HPLC grade) were obtained from Burdick and Jackson (Muskegon, MI). Acetic acid (glacial) was obtained from BDH (Poole, Great Britain).

Trans-nitrosylation reactions in solution were carried out by mixing equivolumes of 1 mM solutions of GSNO and corresponding Cys in water and allowing the reaction to proceed at room temperature for 10 min. Before infusing the reaction mixture into the mass spectrometer, it was diluted 100-fold by 50:50 methanol: water with 1% acetic acid. For H/D exchange experiments, the reaction mixture was diluted a hundredfold by 50:50 acetonitrile:D_2O with 1% acetic acid. Such dilution of S-nitrosocysteine resulted in S-nitrosocysteine-d_4, while dilution of S-nitrosocysteine-d_2 produced S-nitrosocysteine-d_6.

Mass Spectrometry Experiments

All ion-molecule reactions were carried out on a modified commercial LCQ quadrupole ion-trap mass spectrometer (Finnigan MAT, San Jose, CA). Instrument modifications have been described previously [35, 36]. The ion of interest was mass selected and liquid *t*-butylnitrite was infused into the He line at a rate of 10 μL/min, corresponding to a pressure of $\sim 1 \times 10^{-7}$ Torr in the ion trap region. The samples, which were prepared in 50:50 methanol:water with 1% acetic acid added, were introduced into the ESI source of the mass spectrometer at a flow rate of 5 μL/min. The sheath gas, capillary voltage, and temperature were adjusted to ca. 10 arb. units, 3.0 kV and 250 °C, respectively. The CID experiments were performed using standard procedures by mass selecting the desired precursor ion, and then subjecting it to CID using collision energy sufficient to dissociate the majority of the precursor ions.

All high-resolution mass spectrometry experiments were conducted using a commercially available hybrid linear ion trap and Fourier-transform ion cyclotron resonance (FT-ICR) mass spectrometer (Finnigan LTQ-FT, Bremen, Germany), which is equipped with ESI. The ions of interest were mass selected in the linear ion trap using standard procedures and subjected to CID. Fragment ions were transferred to the FT-ICR cell to generate a high-resolution mass spectrum. Positive mode calibration was preformed via the automatic calibration function using the recommended LTQ calibration solution, consisting of caffeine, MRFA, and Ultramark 1621 solution.

Theoretical Methods

Geometry optimizations and electronic energy calculations were performed using the Gaussian 03 molecular modeling package [37]. Structures of minima and transition states were optimized at the B3-LYP level of theory [38, 39] with the 6-311++G(d,p) basis set. In the case of open-shell systems, spin-unrestricted calculations (UB3-LYP) were used. All optimized structures were subjected to vibrational frequency analysis to ensure they corresponded to either true minima (no imaginary frequencies) or transition states (1 imaginary frequency). Intrinsic reaction coordinate (IRC) runs were performed on each transition state, followed by geometry optimizations to ensure that they connected to the appropriate reactant and product ion minima. The final energies used to calculate the potential energy surfaces were corrected with the (U)B3-LYP/6-311++G(d,p) zero-point vibrational energies, (ZPVE), ($E_{reported} = E_{electronic} + E_{zpve}$).

Strategies for Calculating the Global Minima of Various Forms of Cysteine

A candidate structure for each of the various forms of cysteine was first constructed using ChemBio3D Ultra 11.0 and the energy minimized using the minimize energy functionality from the inbuilt MM2 molecular mechanics package. From this 100 high-energy conformers of each respective form of cysteine were sequentially generated by using the molecular dynamics functionality. The parameters used for the molecular mechanics calculations were: Step Interval = 2.0 fs; Frame Interval = 100.0 fs; Terminate After = 200 steps; Heating/Cooling Rate = 5.0 Kcal/atom/ps; and Target Temperature = 500 Kelvin. In addition, several additional candidate structures were manually constructed based on chemical intuition. Each of these structures were optimized at (U)B3-LYP/6-31G(d)//PM3 and the 10 most stable structures were further optimized at the (U)B3-LYP/6-311++G(d,p)//B3-LYP/6-31+G(d,p) level of theory and the lowest energy structure optimized at (U)B3-LYP/6-311++G(d,p).

Results and Discussion

Formation of Protonated S-Nitrosocysteine in the Gas Phase

Here we describe two different methods for generating protonated nitrosocysteine in the gas phase. Method 1 involves allowing protonated cysteine to undergo ion-molecule reactions with *t*-butylnitrite (eq 2). Related reactions of protonated thiols with nitrite esters have been described previously [34].

$$[\text{R-SH} + \text{H}]^+ + \text{tBuONO} \rightleftarrows [\text{RS-NO} + \text{H}]^+ + \text{tBuOH} \quad (2)$$

The gas-phase ion-molecule reaction between the protonated Cys (*m/z* 122) and tBuONO proceeds cleanly. The only major product is the protonated S-nitrosocysteine (*m/z* 151) corresponding to the addition of 29 Da (a loss of H and an addition of NO) to the $CysH^+$. A representative spectrum is shown in Figure 1a. By maintaining a constant neutral concentration while varying the reaction times, kinetic plots were constructed. Analysis of these plots gave a rate constant of 1.5×10^{-11} cm^3 s^{-1}, which corresponds to a reaction efficiency of 0.5%. While a detailed investigation of the mechanism of this transnitrosylation reaction is beyond the scope of the current work, based upon previous gas-phase studies [34], a possible mechanism is shown in Scheme **1**. Thus, protonated cysteine may react to give an initial ion–molecule complex, **1**, which then undergoes proton transfer to form a new ion–molecule complex, **2**. Subsequently, NO^+/H^+ exchange would form complex **3**, which could fragment via proton transfer to yield protonated S-nitrosocysteine.

Method 2 involves allowing cysteine to undergo a transnitrosylation reaction with an NO donor in solution (eq 3), and then subjecting the resultant solution to ESI/MS.

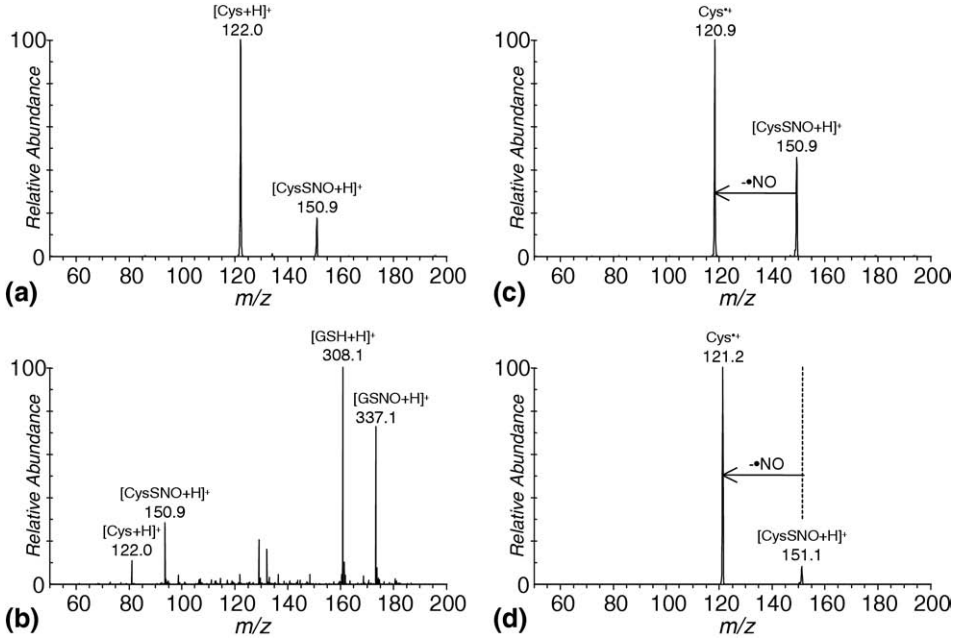

Figure 1. Gas-phase formation and fragmentation of protonated S-Nitrosocysteine. (**a**) LCQ MS^2 spectrum showing the ion-molecule reaction of mass selected protonated cysteine with *t*-butylnitrite (Method 1); (**b**) LTQ ESI/MS of a solution containing cysteine and S-nitrosoglutathione (Method 2); (**c**) LCQ MS^3 CID spectrum of protonated S-Nitrosocysteine formed via Method 1; (**d**) LTQ MS^2 CID spectrum of protonated S-Nitrosocysteine formed via Method 2.

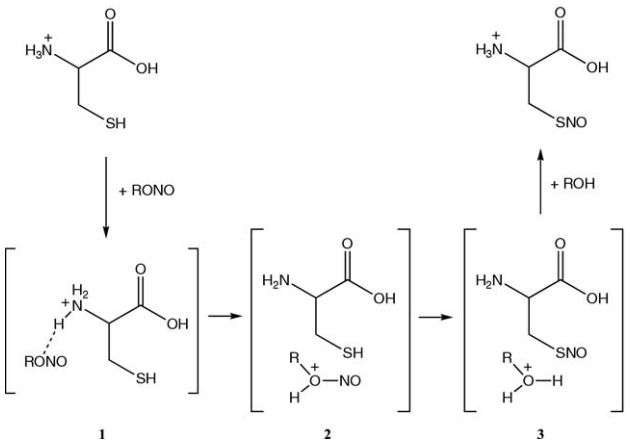

Scheme 1. Possible mechanism for the reaction of protonated cysteine with t-butylnitrite (R = tBu).

$$\text{R-SH} + \text{R'-S-N} = \text{O} \rightleftharpoons \text{R'-SH} + \text{R-S-N} = \text{O} \quad (3)$$

Here R corresponds to Cys, and R′ to the nitrosylating agent (in this case, S-nitrosoglutathione, or GSNO).

The ESI mass spectrum of the reaction mixture resulting from eq 3 is shown in Figure 1b. One can see that an appreciable portion of starting Cys (protonated ion at *m/z* 122) has been converted to S-nitrosocysteine (*m/z* 151). Conversely, a substantial fraction of starting GSNO (protonated ion at *m/z* 337) has been converted to the reduced thiol form GSH (*m/z* 308). Normally, to achieve a higher degree of conversion of Cys to S-NO Cys, a ten- to a 100-fold excess of the nitrosylating agent is used, which drives the equilibrium in reaction (3) to the right as described in our previous studies on S-nitrosylation of model peptides [40]. In this case, however, the excess of GSNO makes it very hard to observe ions of cysteine since the ionization efficiency of the larger glutathione peptide is much higher than that of Cys. Consequently, equimolar quantities of Cys and GSNO were used and the mixture was sprayed without further purification.

Fragmentation of Protonated S-Nitrosocysteine

Fragmentation of protonated S-nitrosocysteine under CID condition results in a very simple spectrum as shown in Figure 1c and d. Both the protonated S-nitrosocysteine formed in the gas-phase by reaction (eq 2), and the one formed in solution by reaction (eq 3) displayed virtually identical MS/MS spectra (cf. Figure 1c and d) including the intensity of the product ion under the same CID conditions. These results, along with their identical MS^3 spectra discussed below, strongly suggest that the same species, protonated S-nitrosocysteine, is formed by these two different processes. The loss of 30 Da, which corresponds to NO, results in the formation of the cysteine radical cation at *m/z* 121 (eq 4, X = NO). Losses of HNO and HONO + CO, which are indicative of N-nitrosoamino acids [41], are not observed. These results are in full agreement with previous studies from our [40] and other [28, 42] groups, which highlighted the labile character of S–NO bond under various MS conditions. In fact, most studies involving S-nitrosylated peptides focus on optimizing the MS conditions to prevent the loss of NO from nitrosylated Cys residues [40, 42]. Numerous approaches have been developed for covalent modification of the nitrosothiol moiety (including the biotin switch assay [43, 44] to avoid the fragmentation of the S-NO bond during MS-based analysis [45, 46]. In this work, we use this facile dissociation to our advantage. This is an example of the violation of the so called "even electron" rule [47] in which bond homolysis occurs for an even electron ion instead of bond heterolysis reactions, which would produce even electron fragments instead. Indeed, the simple replacement of H with NO in cysteine, which changes the S–X bond dissociation energy (BDE), has a profound effect on the types of fragmentation channels which occur. Thus, protonated cysteine (X = H), which has a high S-H BDE (around 91 kcal mol^{-1}) [48], prefers to fragment via the losses of NH_3 (eq 5) and CO and H_2O (eq 6) [49]. In contrast, protonated S-nitrosocysteine (X = NO), which has a low S–NO BDE (around 27 kcal mol^{-1} [50] prefers to fragment via the loss of NO (eq 4).

$$[H_3NCH(CH_2SX)CO_2H]^+ \rightarrow [H_3NCH(CH_2S)CO_2H]^{\bullet +} + \bullet X \quad (4)$$

$$\rightarrow [XSCH_2CHCO_2H]^+ + NH_3 \quad (5)$$

$$\rightarrow [H_2N=CHCH_2X]^+ + CO + H_2O \quad (6)$$

To further examine why bond homolysis (eq 4) outcompetes the even electron fragmentation pathways (eqs 5 and 6), the reaction pathways associated with these three reactions were examined using DFT calculations. From Figure 2 it can be observed that the activation barrier for S–N bond homolysis is lower than those of the two heterolytic reactions corresponding to loss of NH_3 and CO + H_2O losses by 2.5 and 5.2 kcal mol^{-1}, respectively. This is in agreement with the experimental results (Figure 1c and d) whereby exclusive loss of the NO radical occurs. The final product endothermicities are predicted to be 25.3, 33.7, and 24.0 kcal mol^{-1}, respectively. From this it can be said that bond homolysis, which is the sole observable product, occurs as it is kinetically favored even though the CO + H_2O loss is thermodynamically favored. The mechanisms for each of these pathways are described in further detail below (with all associated structures listed in Supplementary Figure S1a, which can be found in the electronic version of this article). All mechanisms occur via S-nitrosocysteine protonated at the amino group, **4a** (Figure 2), which is predicted to be the most stable isomer (Supplementary Table S1 and Supplementary Figure S2).

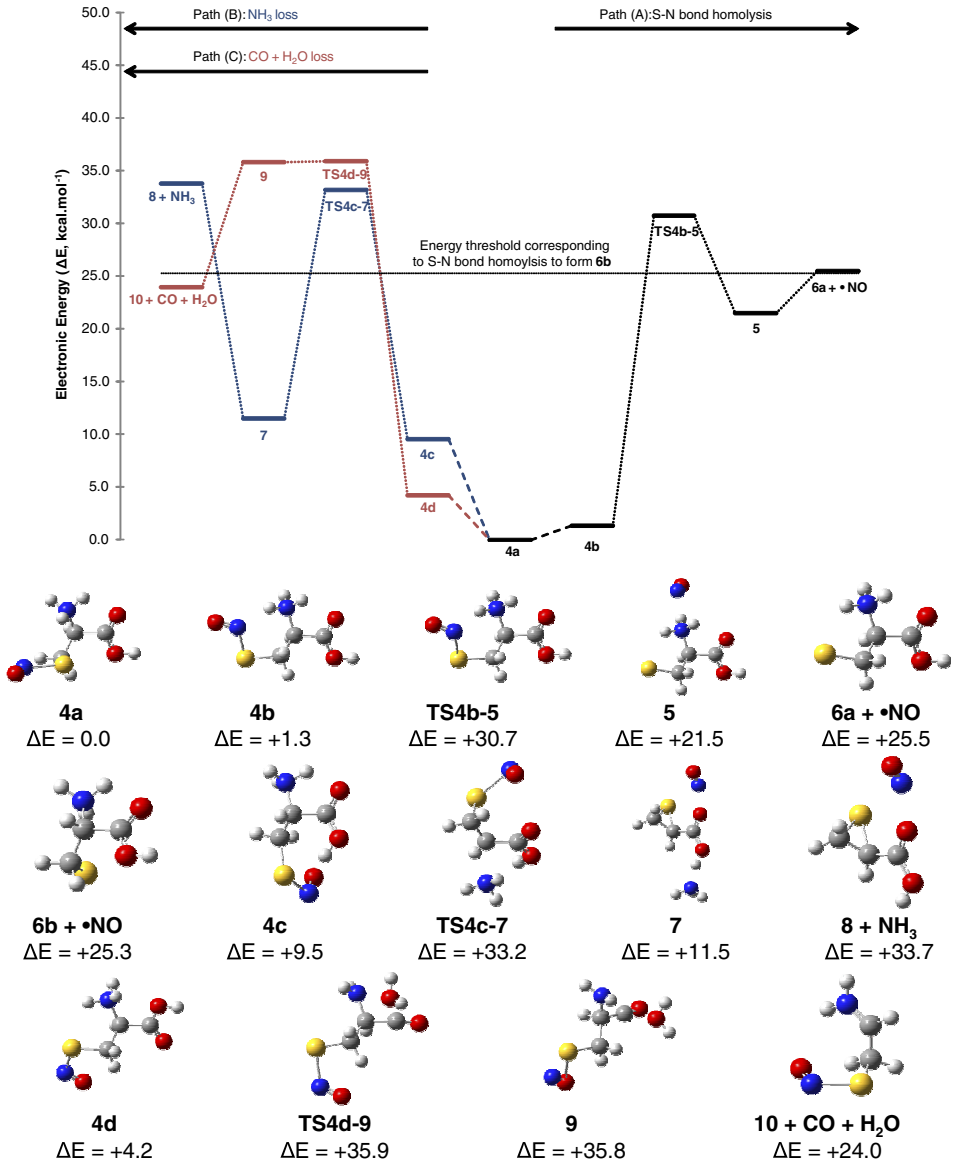

Figure 2. (U)B3-LYP/6-311++G(d,p) calculated reaction pathways and associated structures for key structures involved in the fragmentation of protonated CysNO. Path (**a**): S–N bond-homolysis; Path (**b**): NH_3 loss; and Path (**c**): CO + H_2O loss. For structures and Cartesian coordinates of each species, see Figure S1a of the Supplementary Material. Note that the threshold for •NO loss corresponds to the formation of the most stable rotamer, **6b**.

Homolytic loss of NO from protonated CysNO (eq 4). Formation of the distonic S radical occurs via the loss of the NO radical from the side chain of protonated CysNO. The proposed transition-state (TS) obtained for the homolytic cleavage was calculated for the triplet state. A rigid potential energy surface (PES) scan examining the energy difference relative to the S–N bond length is shown in Supplementary Figure S1b. Attempts at obtaining the singlet state using the Gaussian checkpoint file from the triplet state TS by switching the α HOMO and LUMO orbitals were unsuccessful. The loss of the NO radical is proposed to occur via the conformer **4b** (Figure 2). Homolysis of the S–N bond for the triplet state occurs via transition-state **TS4b-5,** which requires an energy of 30.7 kcal mol^{-1}. Homolysis leads to the triplet state ion–molecule complex **5**, consisting of the cysteine radical cation and the NO radical, which lies 21.5 kcal mol^{-1} above the local minimum. The energy of the final product **6a**, calculated at the singlet state, combined with NO resides at 4.0 kcal mol^{-1} above the ion-molecule complex **5**. A slightly more stable rotamer, **6b**, was found which was used to calculate the endothermicity of the homolysis reaction. Thus the S–NO bond dissociation energy (BDE) of protonated CysNO to give **6b** and •NO is 25.3 kcal mol^{-1}, which is consistent with experimentally derived S–NO BDEs for other neutral compounds [50].

Loss of NH_3 from protonated CysNO (eq 5). The loss of NH_3 (eq 5) from protonated CysNO is most likely to occur via a neighboring group attack by the side chain of cysteine to form a stable episulfonium ion **8**, in an analogous mechanism to that previously described for NH_3 loss from protonated cysteine [49]. This neighboring group pathway is predicted to occur via conformer **4c** which lies 9.5 kcal mol^{-1} above the local minimum, **4a**. The neighboring group attack by the sulfur nucleophile onto the a carbon occurs via transition-state **TS4c-7** with an activation energy of 33.2 kcal mol^{-1}. Separation of the resultant ion-molecule complex **7**, yields the episulfonium ion, **8**, with an endothermicity of 33.7 kcal mol^{-1}. Evidence of the lability of the S–NO bond is demonstrated in this pathway by the lengthening of the S–N bond from the initial 2.04 angstroms in the local minima to 2.27Å in the TS and finally to complete dissociation of the S–NO bond to form complex **7**, which is best described as a triple complex between the NO^+ and thiirane carboxylic acid that is further solvated by NH_3 (via H bonding to the OH of the carboxylic acid functional group). Removal of NH_3 from complex **7** produces complex **8** in which NO^+ is solvated by thiirane carboxylic acid.

Loss of CO and H_2O from protonated CysNO (eq 6). Concurrent loss of CO and H_2O from protonated CysNO is predicted to occur via an intramolecular proton transfer from the amino group onto the hydroxyl group in a mechanism similar to that previously calculated for protonated glycine by Uggerud [51] and O'Hair et al. [49]. Starting from conformer **4d** this proton migration occurs via **TS4d-9** that lies 35.9 kcal mol^{-1} higher in energy than **4a**. An intrinsic reaction coordinate (IRC) search was performed on **TS4d-9** to yield the corresponding ion-molecule complex **9**. Removal of both CO and H_2O from **9**, followed by optimization gave the immonium ion **10**, with an overall endothermicity of 24.0 kcal mol^{-1}.

Experimental Studies on the Fragmentation of the Cysteine Radical Cation

The fragmentation of Cys radical cation by CID proceeded exactly the same way independent of the method used to form the protonated S-nitrosocysteine (either formed in the gas phase or in solution as described above). The major products of $Cys^{\bullet+}$ dissociation correspond to the loss of •COOH (45 Da, eq 8), CH_2S (46 Da, eq 9), $\bullet CH_2SH$ (47 Da, eq. 10), and H_2S (34 Da, eq 11) as shown in Figure 3a. In addition, three different deuterium labeling experiments were carried out to pinpoint the origin of hydrogen atoms in the CID products, and the resulting CID spectra are given in Figure 3b–d. The first experiment involved using commercially available Cys-d_2, where both of the side-chain C–H hydrogens are replaced by deuteriums. The second experiment involved carrying out solution H/D exchange of natural Cys, which produced Cys-$d_4^{\bullet+}$ in which all the labile hydrogens (three in the protonated amino group, and the carboxyl one) were replaced by deuteriums. In the third experiment, solution phase H/D exchange of Cys-d_2 was

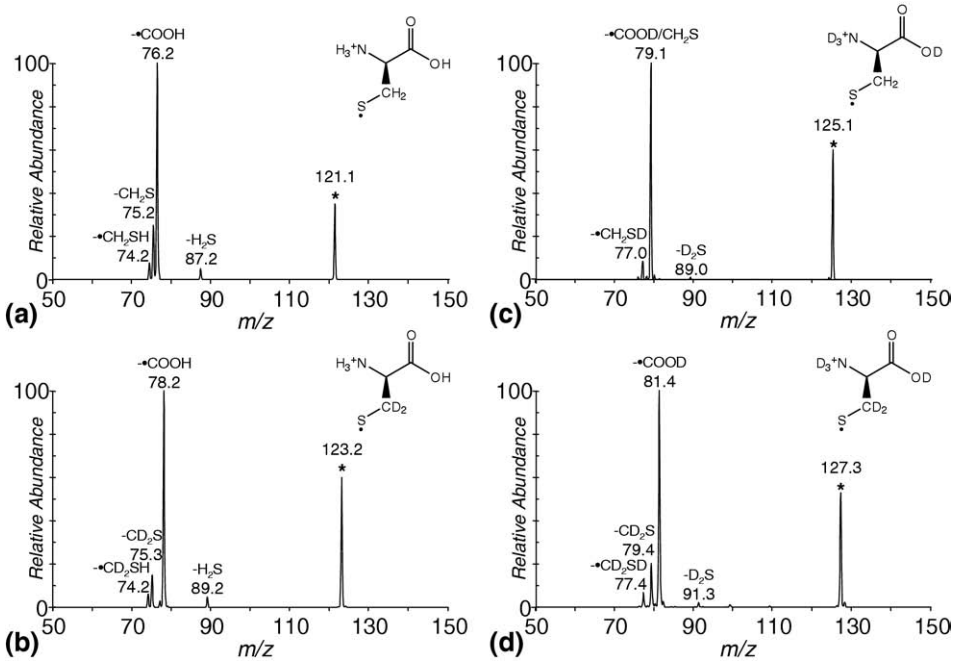

Figure 3. LTQ collision-induced dissociation of radical cations of cysteine. (**a**) $[H_3NCH(CH_2S)CO_2H]^{\bullet+}$; (**b**) $[H_3NCH(CD_2S)CO_2H]^{\bullet+}$; (**c**) $[D_3NCH(CH_2S)CO_2D]^{\bullet+}$; (**d**) $[D_3NCH(CD_2S)CO_2D]^{\bullet+}$. An asterisk refers to the mass-selected precursor ion. Note that for spectrum (**c**), a nested isolation was carried out in which the precursor was first isolated with a 10 Da window followed by reisolation with a 1.5 Da window.

carried out and resulted in Cys-$d_6^{\bullet+}$, in which all hydrogens except the α carbon C–H were replaced by deuteriums. The structures of all these deuterium labeled ions along with their corresponding CID spectra are given in Figure 3b–d, respectively.

$$[H_3NCH(CH_2S)CO_2H]^{\bullet+}$$

$$\rightarrow [H_2N=CH(CH_2SH)]^+ + \bullet COOH \quad (8)$$

$$\rightarrow [H_3NCHCO_2H]^{\bullet+} + CH_2S \quad (9)$$

$$\rightarrow [H_2N=CHCO_2H]^+ + \bullet CH_2SH \quad (10)$$

$$\rightarrow [C_3,H_5,N,O_2]^{\bullet+} + H_2S \quad (11)$$

An examination of the CID spectrum of Cys-$d_2^{\bullet+}$ (*m/z* 123) shown in Figure 3b reveals that both deuteriums are lost as CD_2S (product ion *m/z* 75, loss of 48 Da) and $\bullet CD_2SH$ (product *m/z* 74, loss of 49 Da), confirming that two of the hydrogens originate from the CH_2 group of the side chain of Cys. The loss of H_2S (product ion *m/z* 89, loss of 34 Da) does not involve any D atoms, which means that no side-chain hydrogens are involved in this channel. The loss of •COOH (base peak at *m/z* 78, loss of 45 Da) does not involve any D atoms either. Thus, the side-chain CH_2 hydrogens are not involved in any H/D scrambling reactions, which precede fragmentation. FT-ICR MS high-resolution mass measurements were used to assign the product ions and thereby confirm the formulas associated with these losses (see Supplementary Table S2).

The CID spectrum of Cys-$d_4^{\bullet+}$ (*m/z* 125), in which all labile hydrogen atoms are substituted for deuteriums, is shown in Figure 3c. Here the base peak occurs at *m/z* 79, which corresponds to the losses of •COOD and CH_2S (both nominally 46 Da). The peak at *m/z* 77 results from the loss of $\bullet CH_2SD$ (48 Da). Finally, the smallest peak is at *m/z* 89 and corresponds to the loss of D_2S. Thus, the H_2S loss channel from $Cys^{\bullet+}$ requires that the hydrogens come from labile (originally amino or carboxyl) positions.

Finally, the fragmentation of Cys-$d_6^{\bullet+}$ (Figure 3d) reveals the following: the loss of •COOD (base peak at *m/z* 81, loss of 46 Da); the loss of CD_2S (product ion *m/z* 79, loss of 48 Da); the loss of $\bullet CD_2SD$ (product ion *m/z* 77, loss of 50 Da); and the loss of D_2S (product ion *m/z* 91, loss of 36 Da). This confirms that the hydrogen atom at the α carbon (the only H atom not replaced by D in Cys-$d_6^{\bullet+}$) is not included in any of the neutral loss products, contrary to the theoretical predictions of Zhao and coworkers [32] (this is further discussed below).

A summary of the CID products from all four CID experiments on the cysteine radical cations is given in Table 1. No other products in appreciable quantities were detected in fragmentation of these ions. Special care was taken to look for low-mass (under *m/z* 50) product ions but none were detected.

Potential Mechanisms for the Decomposition Reactions of Long Lived Cysteine Radical Cations

By using the results of the labeling experiments described above together with the three previous theoretical studies [30–32], it is possible to make some comments on potential mechanisms for the fragmentation reactions of the cysteine radical cations. A key feature that has emerged from previous theoretical studies is that various tautomeric forms of the cysteine radical cations may be involved in the different fragmentation reactions, and that these may interconvert via intramolecular proton or H atom transfer reactions. Scheme **2** shows the structures of the tautomeric forms that we have considered and carried out DFT calculations on. The relative energy of each isomer is given below the structure, while the associated cartesian coordinates and energies for these structures are available in Supplementary Figure S3 and Table S3. Not all of these structures appear to be stable, as discussed further below.

An examination of Scheme **2** reveals that the expected CID product of eq 4, the distonic ion **6b**, is not the most stable species, which instead is **14**. Radical cation **11a** is also a distonic ion and is related to **6b** via

Table 1. CID fragmentation losses from the deuterium-labeled cysteine radical cations

Precursor Species	$Cys^{\bullet+}$	Cys-$d_2^{\bullet+}$	Cys-$d_4^{\bullet+}$	Cys-$d_6^{\bullet+}$
S-distonic radical cation structure	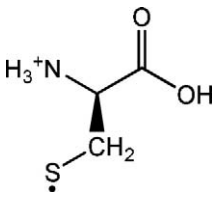	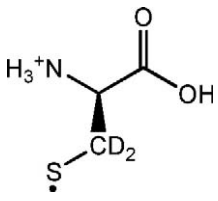	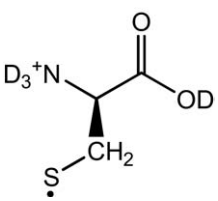	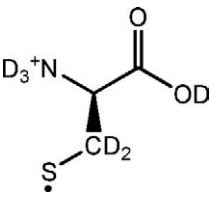
Precursor *m/z*	121	123	125	127
Losses upon CID	−45 (•COOH) −46 (CH_2S) −47 ($\bullet CH_2SH$) −34 (H_2S)	−45 (•COOH) −48 (CD_2S) −49 ($\bullet CD_2SH$) −34 (H_2S)	−46 (•COOD) −46 (CH_2S) −48 ($\bullet CH_2SD$) −36 (D_2S)	−46 (•COOD) −48 (CD_2S) −50 ($\bullet CD_2SD$) −36 (D_2S)

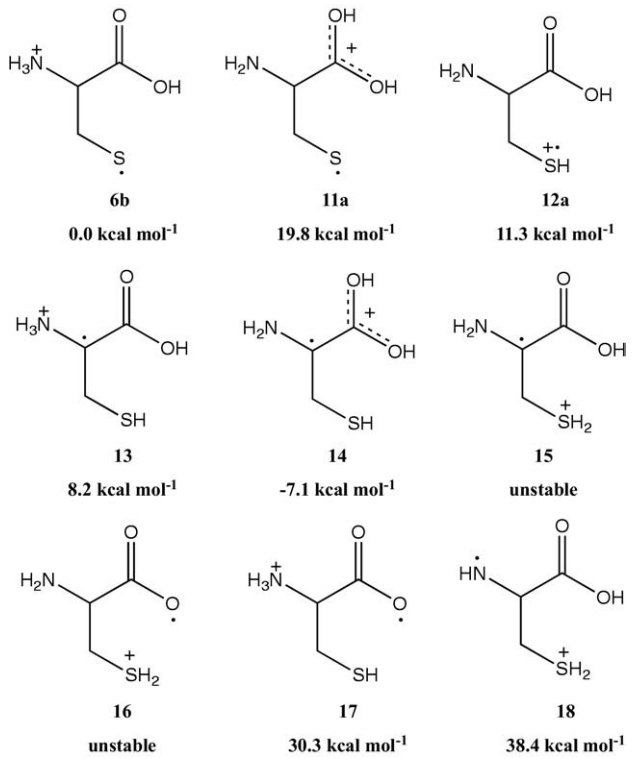

Scheme 2. Isomers of the radical cation of cysteine considered. The relative energies listed below each isomer are from DFT calculations carried out at the UB3-LYP/6-311++G(d,p) level of theory. For structures and Cartesian coordinates of each isomer, see Figure S3 of the supplementary material.

an intramolecular proton transfer from the N to the CO group, and has been considered in a previous theoretical study [32]. The canonical form, **12a**, is directly related to the removal of an electron from the sulfur atom of neutral cysteine and has been examined in all three past theoretical studies [30–32]. An additional structure exists (not shown in Scheme 2) whereby the charge and radical site resides on the nitrogen rather than the sulfur. This structure however is presumed to be higher in energy as indicated by a study on the photoelectron spectra of amino acids carried out by Cannington and Ham [52] whereby ionization from the lone-pair orbitals of sulfur was found to be the lowest energy process. Species **13-15**, formed via H atom transfer from the α C–H to the S, are all related to each other via intramolecular proton transfer. The special stability of **14** has been noted previously by Zhao et al. [32], and is due to the captodative nature of the radical. In contrast, isomer **15** appears to be unstable. Thus an attempted optimization of **15** resulted in the cleavage of the C–S bond to give an ion-molecule complex (IMC) between the radical cation of dehydroalanine and H_2S. Finally, in **16-18**, the radical sites are located at O, O and N respectively. Optimization of **16** resulted in what appears to be a barrierless intramolecular H transfer to yield a rotamer of **12a**, while isomers **17** and **18** are substantially higher in energy. In the next sections, we examine how some of these radical cations are involved in the fragmentation reactions shown in eqs 8–11.

Mechanism for loss of CH_2S (eq 9). Loss of CH_2S is expected to result from a simple C–C bond cleavage reaction, which proceeds directly from either **6d** or **11c** (Figure 4). The barrier for the latter reaction, from **11c**, has been previously calculated to be 30.1 kcal mol^{-1} [32], but apparently the related fragmentation reaction occurring directly from the distonic ion **6d** has not been previously considered. Thus, we have calculated the surfaces associated with both of these mechanisms and the results of these calculations are shown in Figure 4 as: Path (A) loss of CH_2S from **11c**; Path (B) loss of CH_2S from **6d**. Direct fragmentation of **6d** via loss of CH_2S leads to **24**, and this process is endothermic by 39.6 kcal mol^{-1} with a barrier of 45.1 kcal mol^{-1}. In contrast, the pathway through the radical cation **11c** leading to **22** is considerably less endothermic (only 21.6 kcal mol^{-1}) and also has a lower transition-state energy (30.1 kcal mol^{-1}). These calculations suggest that CH_2S loss is much more likely to occur from the radical cation **11c** as originally proposed by Zhao and coworkers [32]. This is an interesting example of how the stability of the product ion dictates the need to tautomerize a distonic ion before a simple radical fragmentation reaction.

Mechanism for losses of •COOH (eq 8) and •CH_2SH (eq 10). Both of the radical losses •COOH (eq 8) and •CH_2SH (eq 10) are expected to be simple alpha cleavage reactions involving the radical cation of the canonical form, to yield the even electron immonium ions $[H_2N = CH(CH_2SH)]^+$ (**20** in Figure 4) and $[H_2N = CHCO_2H]^+$ (**25** in Figure 4). Thus the key first step in the fragmentation pathway must involve an H atom migration from N to S in the precursor **6b**, to give **12b**, which has been calculated to have a barrier of 20.8 kcal mol^{-1}. Zhao and coworkers have previously calculated the energetics for the subsequent endothermic cleavage reactions [32], 28.2 kcal mol^{-1} for the loss of •COOH and 34.6 kcal mol^{-1} for the loss of •CH_2SH; both values are given relative to the energy of precursor **6b**. Gil et al. [31] calculated very similar values, 29.4 and 35.4 kcal mol^{-1}, respectively. Our calculations (available in Supplementary Table S4) concur with this trend, giving the energies of 25.6 and 34.7 kcal mol^{-1}, respectively.

While the loss of •COOH, Path (C) of Figure 4, is more endothermic than the loss of CH_2S via Path (A) (25.6 versus 21.6 kcal mol^{-1}), it is also important to consider the barriers associated with the fragmentation processed occurring in a slow heating dissociation process such as low-energy CID. The highest energy transition state for •COOH loss occurs at 24.8 kcal mol^{-1}, which is *below* the overall reaction endothermicity of 25.6 kcal mol^{-1}. In contrast, the loss of CH_2S via Path (A) has a barrier of 30.1 kcal mol^{-1}, which is *above* the overall reaction endothemicity of 21.6 kcal mol^{-1}. Although we have been unable to locate a transition-state for the loss of •CH_2SH, Path (D) of Figure 4, the

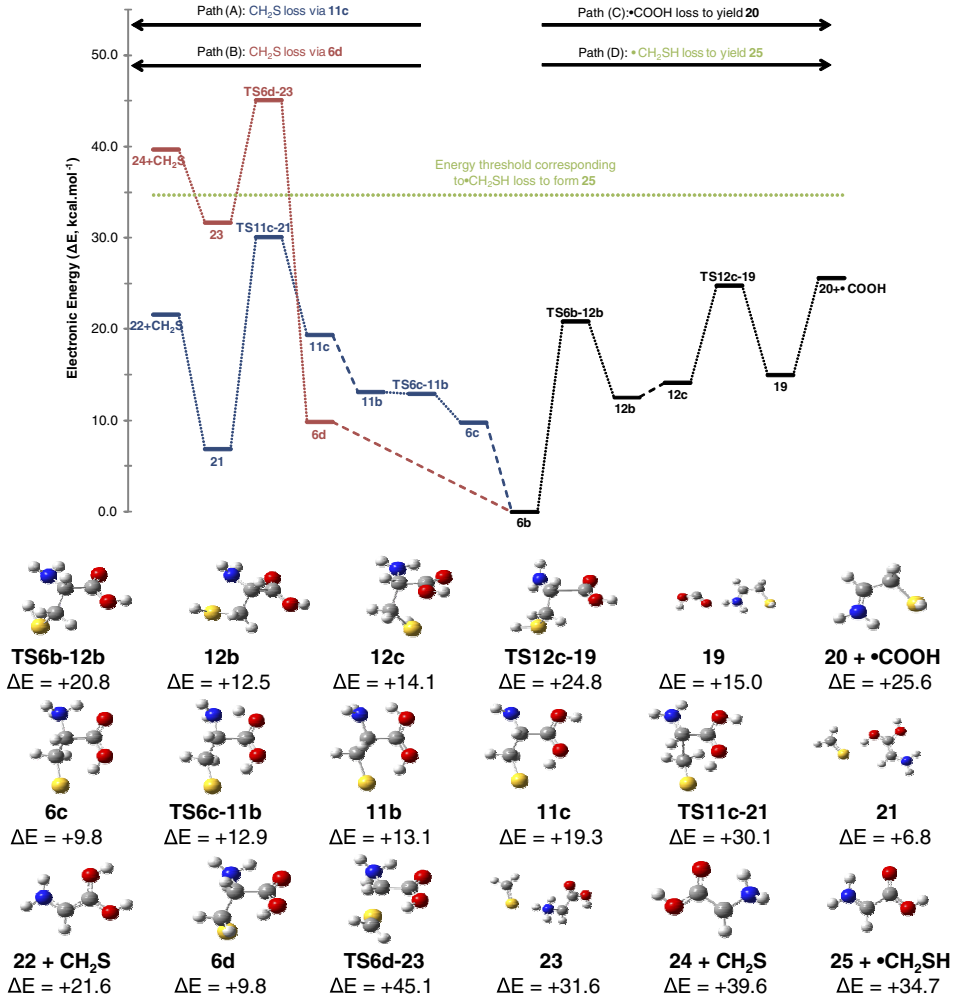

Figure 4. (U)B3-LYP/6-311++G(d,p) calculated reaction pathways and associated structures for key structures involved in the fragmentation of $Cys^{\bullet+}$. Path (**a**) CH_2S loss from **11c**; Path (**b**) CH_2S loss from **6d**; Path (**c**) •COOH loss; and Path (**d**) $\bullet CH_2SH$ loss (only reaction endothermicity shown). For structures and Cartesian coordinates of each species, see Figure S4 of the Supplementary Material.

overall reaction endothemicity (34.7 kcal mol^{-1}) is higher than the energetics associated with Paths (A) and (C). Thus the low-energy CID results are thus consistent with this picture, with the loss of •COOH being the dominant channel followed by the losses of CH_2S and $\bullet CH_2SH$.

Mechanism for loss of H_2S (eq 11). Although loss of H_2S (eq 11) is only a minor channel, it is the most complex of all the reactions as two H atoms need to migrate to sulfur starting from **6b**. Zhao et al. have previously found a transition-state for H_2S loss [32], but this reaction was found to involve the H atom from the α carbon, which is not consistent with the deuterium labeling results shown in Figure 3c and d. Thus, it seemed worthwhile to calculate potential isomers of formula, $[C_3,H_5,N,O_2]^{\bullet+}$, corresponding to the ion arising from loss of H_2S. The structures of these isomers are shown in Scheme **3**. The relative energies of each of these isomers is given in bold in Scheme **3**, while their energies combined with that of H_2S and relative to **6b** (which gives the predicted isomer specific endothermicity for eq 11) are given in italics. Cartesian coordinates of each of the optimized structures are shown in Figure S5 of the Supplementary Material section. From the calculations on potential isomers of $[C_3,H_5,N,O_2]^{\bullet+}$, **26**, which corresponds to the proposed product ion from Zhao et al. [32], emerged as being the most stable. Zhao et al. [32], noted that the transition-state energy associated with the formation of **26** (relative to **6b**) is 29.9 kcal mol^{-1}, which should make this reaction competitive with CH_2S loss. Given the inconsistency with the deuterium labeling experiments, we attempted to find transition states corresponding to loss of H_2S that did not involve the a hydrogen migration (data not shown). Unfortunately an alternative, lower energy pathway could not be found. Thus all other mechanisms considered were higher in energy than the pathway proposed by Zhao et al. [32]. Indeed, the isomers in which the a C–H remains intact (isomers **29**, **31**, and **32** of Scheme **3**)

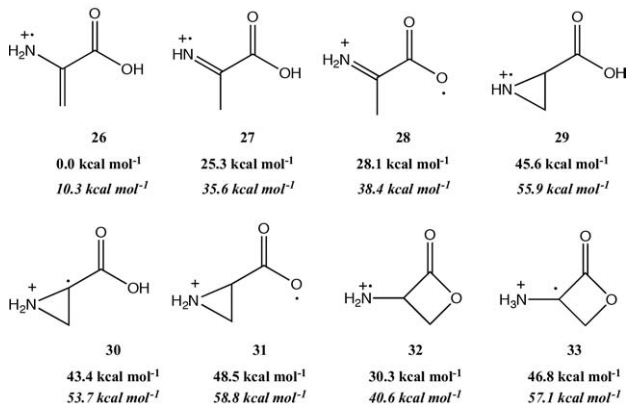

Scheme 3. Potential isomers of formula, $[C_3,H_5,N,O_2]^{\bullet+}$, corresponding to the ion arising from loss of H_2S from the cysteine radical cation. The relative energies listed below each isomer are from DFT calculations carried out at the UB3-LYP/6-311++G(d,p) level of theory. The energies shown in italics correspond to the sum of the isomer + H_2S expressed relative to **6b** (thus representing the endothermicity for eq 11). For structures and Cartesian coordinates of each isomer, see Figure S5 of the Supplementary Material.

are all considerable higher in energy. While we are unable to resolve the discrepancy between the deuterium labeling studies and the DFT calculations, it is worth recalling that the H_2S loss channel is only a minor one.

Conclusions

Protonated S-nitrosocysteine, a precursor to the cysteine radical cation, has been prepared by two different means: gas-phase ion–molecule reaction of protonated cysteine with *t*-butylnitrite; and a transnitrosylation of cysteine in solution by a nitric oxide donor GSNO followed by the transfer of protonated S-nitrosocysteine into the gas phase by ESI-MS. A comparison of the CID spectra of protonated cysteine and S-nitrosocysteine reveals that the simple replacement of H with NO in cysteine has a profound effect on the types of fragmentation channels that occur. Thus, protonated cysteine, which has a high S-H BDE (in the order of 91 kcal mol^{-1}) [48], obeys the even electron rule since it fragments via the losses of NH_3 (eq 5) and CO and H_2O (eq 6) [49]. In contrast, protonated S-nitrosocysteine, which has a low S–NO BDE (in the order of 27 kcal mol^{-1}) [50], violates the even electron rule by fragmenting via the loss of •NO (eq 4). The loss of •NO provides access to a long-lived cysteine radical cation, which fragments under CID via a dominant loss of •COOH (eq 8), with losses of CH_2S (eq 9), •CH_2SH (eq 10), and H_2S (eq 11) being minor channels. DFT calculations suggest that proton and/or H atom migrations precede all of these losses.

Since a wide range of thiols can be converted into nitrosothiols by solution transnitrosylation (eq 3), the facile loss of nitric oxide from the resultant ESI generated protonated nitrosothiols offers an easy and general route to gas-phase S-distonic radical cations. While the detailed gas-phase fragmentation reactions of protonated S-nitrosocysteine and the cysteine radical cation have only been considered in this work, we have been able to form a wide range of radical cations from nitrosylated cysteine derivatives, cysteine containing peptides, and thiols. Future studies will explore the gas-phase chemistry of radical cations prepared via this method.

Acknowledgments

The authors thank the ARC for financial support via the ARC Centre of Excellence in Free Radical Chemistry and Biotechnology. The authors gratefully acknowledge the generous allocation of computing time from both the Victorian Institute for Chemical Science High Performance Computing Facility and the Victorian Partnership for Advanced Computing. The authors thank the ARC and VICS for funding of the LTQ-FT MS instrument. AKYL acknowledges the award of a Melbourne Research Scholarship from The University of Melbourne. VR acknowledges the support from Northern Illinois University and thanks RAJO and The University of Melbourne for research opportunities during his sabbatical leave.

Appendix A Supplementary Material

Supplementary data associated with this article can be found, in the online version, at doi:10.1016/j.jasms.2008.12.026.

References

1. Stubbe, J. Radicals with a Controlled Lifestyle. *Chem. Commun. (Cambridge, U.K.).* **2003,** *20,* 2511–2513.
2. Cadet, J.; Bardet, M.; Berger, M.; Berthod, T.; Delatour, T.; D'Ham, C.; Douki, T.; Gasparutto, D.; Grand, A.; Guy, A.; Jolibois, F.; Molko, D.; Polverelli, M.; Ravanat, J. L.; Romieu, A.; Signorini, N.; Sauvaigo, S. Oxidative Base Damage to DNA: Recent mechanistic Aspects, Measurement, and Repair. *NATO ASI Ser., Ser. A* **1999,** *302,* 47–58.
3. Davies, M. J. The Oxidative Environment and Protein Damage. *Biochim. Biophys. Acta Proteins Proteomics* **2005,** *1703,* 93–109.
4. Barlow, C. K.; O'Hair, R. A. J. Gas-Phase Peptide Fragmentation: How Understanding the Fundamentals Provides a Springboard to Developing New Chemistry and Novel Proteomic Tools. *J. Mass Spectrom.* **2008,** *43,* 1301–1319.
5. Budzikiewicz, H.; Djerassi, C.; Williams, D. H. *Structure Elucidation of Natural Products by Mass Spectrometry. Vol. II: Steroids, Terpenoids, Sugars, and Miscellaneous Classes*; Holder-Day: San Francisco, 1964; p. 1–360.
6. Becker, C. H.; Wu, K. J. On the Photoionization of Large Molecules. *J. Am. Soc. Mass Spectrom.* **1995,** *6,* 883–888.
7. Weinkauf, R.; Schanen, P.; Yang, D.; Soukara, S.; Schlag, E. W. Elementary Processes in Peptides: Electron Mobility and Dissociation in Peptide Cations in the Gas Phase. *J. Phys. Chem.* **1995,** *99,* 11255–11265.
8. Grotemeyer, J.; Schlag, E. W. Peptides Investigated by Laser Desorption-Multiphoton Ionization Mass Spectrometry. Part VII. *Org. Mass Spectrom.* **1988,** *23,* 388–396.
9. Cui, W.; Hu, Y.; Lifshitz, C. Time Resolved Photodissociation of Small Peptide Ions. Combining Laser Desorption with Ion Trap/Reflectron TOF Mass Spectrometry. *Eur. Phys. J. D.* **2002,** *20,* 565–571.
10. Sheu, S. Y.; Yang, D. Y.; Selzle, H. L.; Schlag, E. W. Charge Transport in a Polypeptide Chain. *Eur. Phys. J. D.* **2002,** *20,* 557–563.
11. Hu, Y.; Hadas, B.; Davidovitz, M.; Balta, B.; Lifshitz, C. Does IVR Take Place Prior to Peptide Ion Dissociation? *J. Phys. Chem. A* **2003,** *107,* 6507–6514.
12. Zubarev, R. A.; Kelleher, N. L.; McLafferty, F. W. Electron Capture Dissociation of Multiply Charged Protein Cations. A Nonergodic Process. *J. Am. Chem. Soc.* **1998,** *120,* 3265–3266.
13. Iavarone, A. T.; Paech, K.; Williams, E. R. Effects of Charge State and Cationizing Agent on the Electron Capture Dissociation of a Peptide. *Anal. Chem.* **2004,** *76,* 2231–2238.
14. Turecek, F. N–Cα Bond Dissociation Energies and Kinetics in Amide and Peptide Radicals. Is the Dissociation a Nonergodic Process? *J. Am. Chem. Soc.* **2003,** *125,* 5954–5963.

15. Syrstad, E. A.; Turecek, F. Toward a General Mechanism of Electron Capture Dissociation. *J. Am. Soc. Mass Spectrom.* **2005,** *16,* 208–224.
16. McLuckey, S. A.; Goeringer, D. E. Slow Heating Methods in Tandem Mass Spectrometry. *J. Mass Spectrom.* **1997,** *32,* 461–474.
17. Chu, I. K.; Rodriquez, C. F.; Lau, T.-C., Hopkinson, A. C.; Siu, K. W. M. Molecular Radical Cations of Oligopeptides. *J. Phys. Chem. B* **2000,** *104,* 3393–3397.
18. Hopkinson, A. C.; Siu, K. W. M. Peptide radical cations. In *Principles of Mass Spectrometry Applied to Biomolecules,* Laskin, J.; Lifshitz, C., Eds.; John-Wiley & Sons, Inc.: Hoboken, NJ, 2006; p. 301–335.
19. Barlow, C. K.; McFadyen, W. D.; O'Hair, R. A. J. Gas-Phase Ion Chemistry of Biomolecules. Part 44. Formation of Cationic Peptide Radicals by Gas-Phase Redox Reactions with Trivalent Chromium, Manganese, Iron, and Cobalt Complexes. *J. Am. Chem. Soc.* **2005,** *127,* 6109–6115.
20. Laskin, J.; Futrell, J. H.; Chu, I. K. Is Dissociation of Peptide Radical Cations an Ergodic Process? *J. Am. Chem. Soc.* **2007,** *129,* 9598–9599.
21. Laskin, J.; Yang, Z.; Lam, C.; Chu, I. K. Charge-Remote Fragmentation of Odd-Electron Peptide Ions. *Anal. Chem. (Washington, DC).* **2007,** *79,* 6607–6614.
22. Laskin, J.; Yang, Z.; Chu, I. K. Energetics and Dynamics of Electron Transfer and Proton Transfer in Dissociation of MetalIII(salen)–Peptide Complexes in the Gas Phase. *J. Am. Chem. Soc.* **2008,** *130,* 3218–3230.
23. Yang, Z.; Lam, C.; Chu, I. K.; Laskin, J. The Effect of the Secondary Structure on Dissociation of Peptide Radical Cations: Fragmentation of Angiotensin III and Its Analogues. *J. Phys. Chem. B* **2008,** *112,* 12468–12478.
24. Hodyss, R.; Cox, H. A.; Beauchamp, J. L. Bioconjugates for Tunable Peptide Fragmentation: Free Radical Initiated Peptide Sequencing (FRIPS). *J. Am. Chem. Soc.* **2005,** *127,* 12436–12437.
25. Chacon, A.; Masterson, D. S.; Yin, H.; Liebler, D. C.; Porter, N. A. N-Terminal Amino Acid Side-Chain Cleavage of Chemically Modified Peptides in the Gas Phase: A mass Spectrometry Technique for N-Terminus Identification. *Bioorg. Med. Chem.* **2006,** *14,* 6213–6222.
26. Masterson, D. S.; Yin, H.; Chacon, A.; Hachey, D. L.; Norris, J. L.; Porter, N. A. Lysine Peroxycarbamates: Free Radical-Promoted Peptide Cleavage. *J. Am. Chem. Soc.* **2004,** *126,* 720–721.
27. Wee, S.; Mortimer, A.; Moran, D.; Wright, A.; Barlow, C. K.; O'Hair, R. A. J.; Radom, L.; and Easton, C. J. Gas-Phase Regiocontrolled Generation of Charged Amino Acid and Peptide Radicals. *Chem. Commun. (Cambridge, U.K.).* **2006,** *40,* 4233–4235.
28. Hao, G.; Gross, S. S. Electrospray Tandem Mass Spectrometry Analysis of S- and N-Nitrosopeptides: Facile Loss of NO and Radical-Induced Fragmentation. *J. Am. Soc. Mass Spectrom.* **2006,** *17,* 1725–1730.
29. Schoeneich, C. Mechanisms of Protein Damage Induced by Cysteine Thiyl Radical Formation. *Chem. Res. Toxicol.* **2008,** *21,* 1175–1179.
30. Simon, S.; Gil, A.; Sodupe, M.; Bertran, J. Structure and Fragmentation of Glycine, Alanine, Serine, and Cysteine Radical Cations. A Theoretical Study. *J. Mol. Struct.* **2005,** *727,* 191–197.
31. Gil, A.; Simon, S.; Rodriguez-Santiago, L.; Bertran, J.; Sodupe, M. Influence of the Side Chain on the Structure and Fragmentation of Amino Acid Radical Cations. *J. Chem. Theory Comput.* **2007,** *3,* 2210–2220.
32. Zhao, J.; Siu, K. W. M.; Hopkinson, A. C. The Cysteine Radical Cation: Structures and Fragmentation Pathways. *Phys. Chem., Chem. Phys.* **2008,** *10,* 281–288.
33. Barlow, C. K.; Moran, D.; Radom, L.; McFadyen, W. D.; O'Hair, R. A. J. Gas-Phase Ion Chemistry of biomolecules. Part 49. Metal-Mediated Formation of Gas-Phase Amino Acid Radical Cations. *J. Phys. Chem. A* **2006,** *110,* 8304–8315.
34. Gerbaux, P.; Wantier, P.; Flammang, R. Nitrosation of Thiols and Thioethers in the Gas Phase: A Combined Theoretical and Experimental Study. *J. Am. Soc. Mass Spectrom.* **2004,** *15,* 344–355.
35. Reid, G. E.; O'Hair, R. A. J.; Styles, M. L.; McFadyen, W. D.; Simpson, R. J. Gas Phase Ion-Molecule Reactions in a Modified Ion Trap: H/D Exchange of Noncovalent Complexes and Coordinatively Unsaturated Platinum Complexes. *Rapid Commun. Mass Spectrom.* **1998,** *12,* 1701–1708.
36. Waters, T.; O'Hair, R. A. J.; Wedd, A. G. Catalytic Gas Phase Oxidation of Methanol to Formaldehyde. *J. Am. Chem. Soc.* **2003,** *125,* 3384–3396.
37. Frisch, M. J.; Trucks, G. W.; Schlegel, H. B.; Scuseria, G. E.; Robb, M. A.; Cheeseman, J. R.; Montgomery, J.; J. A., Vreven, T.; Kudin, K. N.; Burant, J. C.; Millam, J. M.; Iyengar, S. S.; Tomasi, J.; Barone, V.; Mennucci, B.; Cossi, M.; Scalmani, G.; Rega, N.; Petersson, G. A.; Nakatsuji, H.; Hada, M.; Ehara, M.; Toyota, K.; Fukuda, R.; Hasegawa, J.; Ishida, M.; Nakajima, T.; Honda, Y.; Kitao, O.; Nakai, H.; Klene, M.; Li, X.; Knox, J. E.; Hratchian, H. P.; Cross, J. B.; Bakken, V.; Adamo, C.; Jaramillo, J.; Gomperts, R.; Stratmann, R. E.; Yazyev, O.; Austin, A. J.; Cammi, R.; Pomelli, C.; Ochterski, J. W.; Ayala, P. Y.; Morokuma, K.; Voth, G. A.; Salvador, P.; Dannenberg, J. J.; Zakrzewski, V. G.; Dapprich, S.; Daniels, A. D.; Strain, M. C.; Farkas, O.; Malick, D. K.; Rabuck, A. D.; Raghavachari, K.; Foresman, J. B.; Ortiz, J. V.; Cui, Q.; Baboul, A. G.; Clifford, S.; Cioslowski, J.; Stefanov, B. B.; Liu, G.; Liashenko, A.; Piskorz, P.; Komaromi, I.; Martin, R. L.; Fox, D. J., Keith, T.; Al-Laham, M. A.; Peng, C. Y.; Nanayakkara, A.; Challacombe, M.; Gill, P. M. W.; Johnson, B.; Chen, W.; Wong, M. W.; Gonzalez, C.; Pople, J. A. *Gaussian 03,* Revision B, 04; Gaussian, Inc.: Wallingford, CT, 2004.
38. Becke, A. D. Density-Functional Thermochemistry. III. The Role of Exact exchange. *J. Chem. Phys.* **1993,** *98,* 5648–5652.
39. Lee, C.; Yang, W.; Parr, R. G. Development of the Colle-Salvetti Correlation Energy Formula into a Functional of the Electron Density. *Phys. Rev. B Condens. Matter* **1988,** *37,* 785–789.
40. Taldone, F. S.; Tummala, M.; Goldstein, E. J.; Ryzhov, V.; Ravi, K.; Black, S. M. Studying the S-Nitrosylation of Model Peptides and eNOS Protein by Mass Spectrometry. *Nitric Oxide* **2005,** *13,* 176–187.
41. Freitas, M. A.; O'Hair, R. A. J.; Schmidt, J. A. R.; Tichy, S. E.; Plashko, B. E. Gas-Phase Reactions of Glycine, Alanine, Valine, and Their N-Methyl Derivatives with the Nitrosonium ion, NO+. *J. Mass Spectrom.* **1996,** *31,* 1086–1092.
42. Wang, Y.; Liu, T.; Wu, C.; Li, H. A Strategy for Direct Identification of Protein S-Nitrosylation Sites by Quadrupole Time-of-Flight Mass Spectrometry. *J. Am. Soc. Mass Spectrom.* **2008,** *19,* 1353–1360.
43. Jaffrey, S. R.; Snyder, S. H. The Biotin Switch Method for the Detection of S-Nitrosylated Proteins. *Sci STKE.* **2001,** *2001,* PL1.
44. Jaffrey, S. R.; Erdjument-Bromage, H.; Ferris, C. D.; Tempst, P.; Snyder, S. H. Protein S-Nitrosylation: A Physiological Signal for Neuronal Nitric Oxide. *Nat. Cell Biol.* **2001,** *3,* 193–197.
45. Tummala, M.; Ryzhov, V.; Ravi, K.; Black, S. M. Identification of the Cysteine Nitrosylation Sites in Human Endothelial Nitric Oxide Synthase. *DNA Cell Biol.* **2008,** *27,* 25–33.
46. Hao, G.; Derakhshan, B.; Shi, L.; Campagne, F.; Gross, S. S. SNOSID, a Proteomic Method for Identification of Cysteine S-Nitrosylation Sites in Complex Protein Mixtures. [Erratum to document cited in CA144:346315]. *Proc. Natl. Acad. Sci. U.S.A.* **2006,** *103,* 5242 and references therein.
47. Karni, M.; Mandelbaum, A. The 'Even-Electron Rule'. *Org. Mass Spectrom.* **1980,** *15,* 53–64.
48. McMillen, D. F.; Golden, D. M. Hydrocarbon Bond Dissociation Energies. *Annu. Rev. Phys. Chem.* **1982,** *33,* 493–532.
49. O'Hair, R. A. J.; Styles, M. L.; Reid, G. E. Role of the Sulfhydryl Group on the Gas Phase Fragmentation Reactions of Protonated Cysteine and Cysteine-Containing Peptides. *J. Am. Soc. Mass Spectrom.* **1998,** *9,* 1275–1284.
50. Lue, J.-M.; Wittbrodt, J. M.; Wang, K.; Wen, Z.; Schlegel, H. B.; Wang, P. G.; Cheng, J.-P. NO Affinities of S-Nitrosothiols: A Direct Experimental and Computational Investigation of RS–NO Bond Dissociation Energies. *J. Am. Chem. Soc.* **2001,** *123,* 2903–2904.
51. Uggerud, E. The Unimolecular Chemistry of Protonated Glycine and the Proton Affinity of Glycine. A Computational Model. *Theor. Chem. Acc.* **1997,** *97,* 313–316.
52. Cannington, P. H.; Ham, N. S. The Photoelectron Spectra of Amino Acids: A Survey. *J. Electron. Spectrosc. Relat. Phenom.* **1979,** *15,* 79–82.